Lower limb in sprinters with larger relative mass but not larger normalized moment of inertia

Natsuki Sado[1, 2*], Hoshizora Ichinose[3], Yasuo Kawakami[2]
[1] Faculty of Health and Sports Science, University of Tsukuba, Tsukuba, Japan
[2] Faculty of Sports Sciences, Waseda University, Tokorozawa, Japan
[3] Graduate School of Sport Sciences, Waseda University, Tokorozawa, Japan

Corresponding author:

Natsuki Sado
E-mail: sado.natsuki.gm@u.tsukuba.ac.jp

ORCiDs:

Natsuki Sado: 0000-0002-3958-8193
Yasuo Kawakami: 0000-0003-0588-4039

Author Contributions:

Natsuki Sado: Conceptualization, Data curation, Formal analysis, Investigation, Methodology, Project administration, Visualization, Writing - original draft, Writing – review and editing;
Hoshizora Ichinose: Data curation, Writing – review and editing;
Yasuo Kawakami: Conceptualization, Writing – review and editing

Conflict of interest statement:

There are no conflicts of interest to declare.

Funding:

Yamaha motor foundation for sports to N.S. and JSPS KAKENHI Grant-in-Aid for Young Scientists (21K17592) to N.S.

Keywords:

Biomechanics; Morphology; Adaptation; MRI; Dixon;

Abstract

Inhomogeneous muscle hypertrophy in response to daily motor executions is a morphological adaptation in humans. Morphological adaptation would change the mass distribution, which may affect the mechanical difficulty in moving from an inertia perspective; however, the morphological adaptation from the inertia perspective has not been examined. Here, we show no corresponding differences in the normalized mass and normalized moment of inertia between the sprinters (n=11, 100 m PB: 10.44–10.83 s) and the untrained non-sprinters (n=12) using the fat- and water-separated magnetic resonance images. The lower-limb relative mass was significantly larger in sprinters (18.7±0.7% body mass) than in non-sprinters (17.6±0.6% body mass), while the normalized lower-limb moment of inertia around the hip was similar between them (0.044±0.002 vs. 0.042±0.002 [a. u.]). The thigh relative mass in sprinters (12.9±0.4%) was significantly larger than that in non-sprinters (11.9±0.4%), whereas the shank and foot relative masses were similar. We revealed that the adaptation to sprinting in humans does not relatively increase the mechanical difficulty to swing the lower limb in terms of inertia, even though the lower-limb mass increases reflecting muscular hypertrophy. This is suggested to be one of the significant advantages of human morphology for adaptability to explosive motor tasks.

Introduction

Human morphological characteristics are mainly the result of adaptation to bipedal locomotion (Bramble and Lieberman, 2004; Young et al., 2010). Human morphology enables bipedal walking and endurance running efficiency, resulting in current humans being good endurance runners but poor sprinters (Bramble and Lieberman, 2004). Alternately, evolution in humans has left a great plasticity, allowing them to become faster sprinters via training; for example, the Japan National Record of 50 m sprint is 5.75 s while the average time of 50-m sprint in Japanese males is approximately 7.37±0.52 s (Japan Sports Agency, 2021).

Adaptability in humans has been approached from the muscle morphologies in athletes, based on the exertion abilities of the joint torque (Fukunaga et al., 2001) and power (O'Brien et al., 2009) is primarily determined by the muscle size, especially muscle volume (Balshaw et al., 2021; Fukunaga et al., 2001). Previous MRI studies on sprinters have demonstrated hypertrophy of the trunk and lower-limb muscles (Ema et al., 2018; Miller et al., 2020; Tottori et al., 2021). The hypertrophy was shown to be inhomogeneous with the specific development of the hip flexors and extensors (Ema et al., 2018; Miller et al., 2020; Tottori et al., 2021). The muscle sizes of the hip extensors and flexors are related to the running velocity and/or 100 m sprint time in sub-elite (Ema et al., 2018; Takahashi et al., 2021; Tottori et al., 2021) and elite sprinters (Miller et al., 2020). It has also been reported that the hip extensors' volumes discriminate elite sprinters from the sub-elite (Miller et al., 2020). The muscularity in sprinters reflects the musculoskeletal demands that increasing running velocity in the high-speed range (>7 m/s) requires like the larger torque/power exertion of hip flexors and extensors (Dorn et al., 2012; Schache et al., 2011).

From a mechanical perspective, any motion ($\boldsymbol{a}$:acceleration, $\boldsymbol{\alpha}$:angular acceleration,) is determined by the combination of force-related ($\boldsymbol{f}$: forces, $\boldsymbol{\tau}$: torques) and inertia-related (m: mass, $\boldsymbol{I}$: moment of inertia) factors in line with Newton-Euler equations of motion:

$$m\boldsymbol{a} = \sum \boldsymbol{f}, \tag{1}$$

$$\boldsymbol{I}\boldsymbol{\alpha} = \sum \boldsymbol{\tau}. \tag{2}$$

As humans control their motion via joint torques induced by muscle forces, the relationship between the torque and moment of inertia (Eq. 2) is particularly important for human motor execution. The above muscular characteristics in sprinters (Ema et al., 2018; Miller et al., 2020; Takahashi et al., 2021; Tottori et al., 2021) can be interpreted as an adaptation to force-related factors, but simultaneously, the

morphological changes would involve changes in the mass distribution and thereby inertia-properties. As lean tissue density is larger than that of fat tissue (Huang and Wu, 1976; Martin et al., 1989), the muscular hypertrophy would involve an increase in the lower-limb mass, leading to a general speculation of the trade-off between greater torque exertion ability and greater difficulty in moving the lower limb (i.e., moment of inertia). However, as discussed above, the muscle hypertrophy in sprinters (Ema et al., 2018; Miller et al., 2020; Tottori et al., 2021) is inhomogeneous. This leads to our hypothesis that the mechanical difficulties in swinging the lower limb and the moment of inertia around the hip might not correspond to an increase in the lower-limb mass in sprinters. Anatomists have previously developed scaling coefficients to calculate body segment inertia parameters (BSIPs) for motion analysis. This is done using the direct measurements of elderly cadavers (Clauser et al., 1969) and indirect measurements *in vivo* through medical images or surface scans such as gamma-ray scanning (de Leva, 1996) computed tomography (Huang and Suarez, 1983), magnetic resonance imaging (MRI) (Cheng et al., 2000; Mungiole and Martin, 1990) and three-dimensional laser scanners (Shan and Bohn, 2003). However, the effects of adaptation to motor experience on inertial properties have not been fully examined.

Based on the simple mechanical law shown in Eq. 2), an increase in the moment of inertia leads to (I) increasing musculoskeletal mechanical loads if the motion is consistent, and (II) decreasing angular acceleration if the joint torque exertions are consistent. Understanding the morphological adaptation from an inertial perspective would provide useful knowledge for human motor performance development from both the injury prevention and performance improvement perspectives. In this study, we examined the inertia properties of sprinters by analyzing water- and fat-separated MRIs. Among the inertial properties, we focused on the normalized lower-limb moment of inertia around the hip joint ($\hat{I}^{\mathrm{Hip}}_{\mathrm{LowerLimb}}$) because of the high musculoskeletal demands in the lower limb swing during sprinting (Dorn et al., 2012; Schache et al., 2011).

Results

The body size parameters in sprinters were significantly larger than those in non-sprinters (all $p<0.01$, $d=1.60$, 2.16; Table 1). The absolute values of the lower-limb mass and moment of inertia were significantly correlated to the body size parameters, while the relative mass and $\hat{I}^{\mathrm{Hip}}_{\mathrm{LowerLimb}}$ were not (Fig. 1).

Table 1. Characteristics of participants.

Variable	Sprinters	Non-sprinters
n	11	12
Age [years]	20 ± 2	23 ± 3
Height [cm]	176.7 ± 5.7	168.9 ± 3.9
Mass [kg]	68.2 ± 4.4	58.6 ± 4.5
Leg length [cm]	87.6 ± 4.5	82.7 ± 2.9
$d_{\text{HJC-to-KJC}}$ [cm]	44.1 ± 1.9	41.6 ± 1.6
$d_{\text{KJC-to-AJC}}$ [cm]	37.8± 2.3	35.4 ± 1.3
$d_{\text{Cal-to-MH1–MH5midpoint}}$ [cm]	14.4 ± 0.5	13.6 ± 0.5
$d_{\text{HJC-to-ThighCoM}}$ [cm]	19.4 ± 0.8	18.3 ± 7.4
$d_{\text{HJC-to-ShankCoM}}$ [cm]	59.5 ± 2.8	56.1 ± 2.1
$d_{\text{HJC-to-FootCoM}}$ [cm]	86.6 ± 4.3	81.6 ± 2.9

Note: Data are shown as means ± standard deviations. *n*: the number of participants in each group; $d_{\text{a-to-b}}$: distance from a-to-b in the entire hypothetically constructed lower limb; HJC: Hip joint center; KJC: Kip joint center; AJC: Ankle joint center; Cal: Calcaneus; MH1 (5): 1st (5th) Metatarsal Heads; CoM: Center of mass;

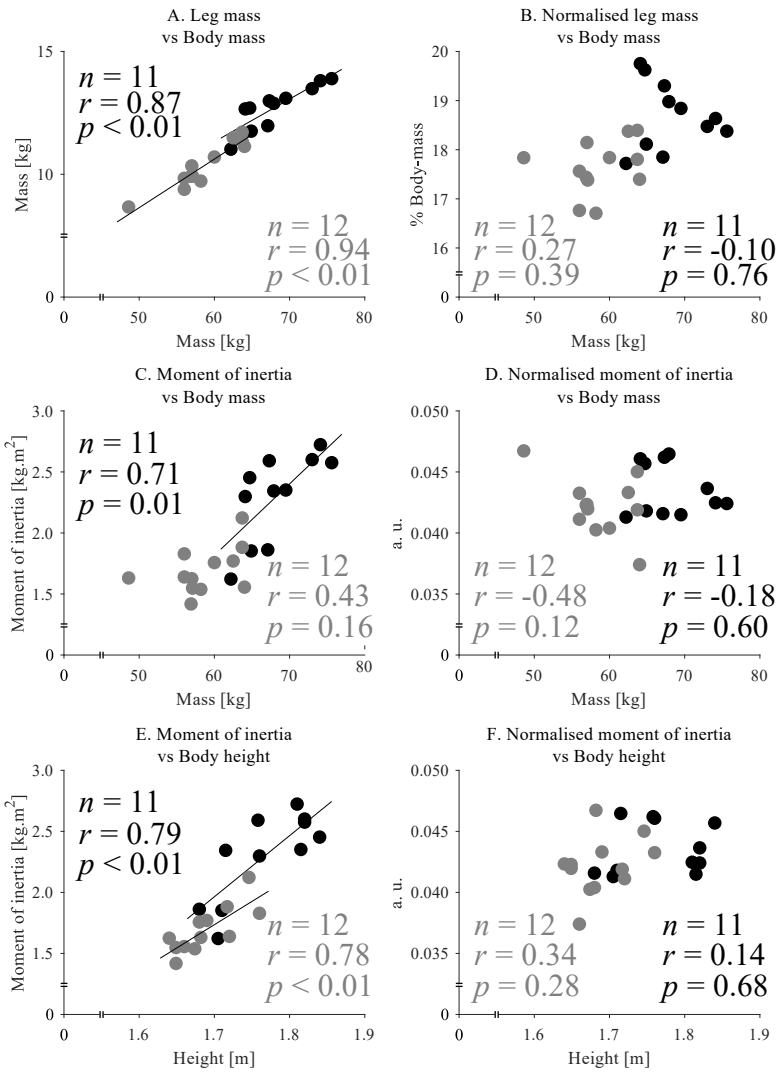

Fig. 1. Relationships between absolute (A, C, E: left column) and normalized (B, D, F: right column) inertia parameters and body size parameters (A–D: body mass, E–F: body height) in sprinters (black) and non-sprinters (gray). Note: *n*, and *r* were the sample size and Pearson's correlation coefficients in each group, respectively.

The relative mass of the entire lower limb was larger in sprinters (18.7±0.7% body mass) than in non-sprinters (17.6±0.6% body mass) (p<0.01, d=1.73; Fig. 2A). However, $\hat{I}^{\mathrm{Hip}}_{\mathrm{LowerLimb}}$ in sprinters (0.044±0.002 [a. u.]) and non-sprinters (0.042±0.002 [a. u.]) did not differ significantly (p=0.15, d=0.62; Fig. 2B). From individual plots, we can observe that, although one of the non-sprinters showed a small $\hat{I}^{\mathrm{Hip}}_{\mathrm{LowerLimb}}$ (Fig. 2B), the $\hat{I}^{\mathrm{Hip}}_{\mathrm{LowerLimb}}$ in non-sprinters and sprinters, except for him, were highly comparable.

The relative thigh mass was significantly larger in sprinters (12.9±0.4%) than in non-sprinters (11.9±0.5%) (p<0.01, d=2.01), while those in the shank (4.5±0.3% vs 4.3±0.3%) and foot (1.4±0.1% vs1.4±0.1%) were similar between them (p=0.13, 0.61, d=0.67, 0.22; Fig. 3A). Compared to non-sprinters, all lower-limb segments in sprinters had a significantly larger lean mass ratio (thigh: 81.7±2.0% vs 72.0±4.8%; shank: 73.0±2.0% vs 66.9±3.1%; foot: 52.3±2.5% vs 48.3±1.9%; all p<0.01, d=1.85–2.62) and smaller fat mass ratio (thigh: 10.3±2.1% vs 19.2±5.6%; shank: 10.2±2.7% vs 15.3±3.5%; foot: 19.6±1.6% vs 24.0±2.5%; all p<0.01, d=1.64–2.09) (Fig. 3B). The mass ratio of the bone tissue in the thigh was smaller in sprinters (8.1±0.6%) than in non-sprinters (8.9±1.1%) (p=0.03, d=1.00; Fig. 3C), while those in the shank and foot were similar between the groups (p=0.24, 0.72, d=0.51, and 0.15; Fig. 3B). The densities of all lower-limb segments were significantly larger in sprinters than in non-sprinters (thigh: 1.064±0.004 g/cm^3 vs1.049±0.012 g/cm^3; shank: 1.084±0.007 g/cm^3 vs1.073±0.008 g/cm^3; foot: 1.061±0.003 g/cm^3 vs. 1.051±0.008 g/cm^3) (all p<0.01, d=1.29–1.60; Fig. 3C). We showed the complete scaling coefficients to calculate the lower-limb segment inertia parameters for sprinters and non-sprinters in Table 2. The radii of gyration, the moment of inertia normalized by the segment length, and segment mass around the segmental mediolateral axis in the thigh (27.7±0.3% vs 27.9±0.2%; p=0.02, d=1.08) and shank (27.0±0.3% vs. 27.6±0.3%; p<0.01, d=2.24) were significantly smaller in sprinters than in non-sprinters.

For the values relating to the examiner's manual processing (digitizing of the anatomical landmarks on MRIs), we confirmed the excellent repeatability in segment lengths with the intraclass correlation coefficients (ICCs) and coefficient of variation (CVs) of 0.993 and 0.01–0.36% for the thigh, 0.994 and 0.00–0.57% for the shank, and 0.963 and 0.17–1.44% for the foot.

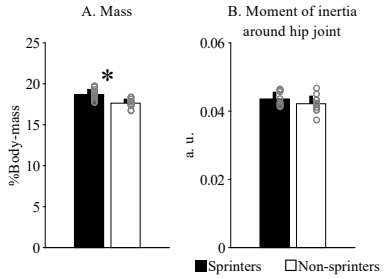

Fig. 2. Whole lower-limb inertia properties. Relative mass (A) and normalized moment of inertia around the hip joint in hypothetically constructed anatomical position data (B). Note: Bar graphs show means and standard deviations. Gray plots show individual data. Asterisk (*) indicates a significant difference between sprinters and non-sprinters.

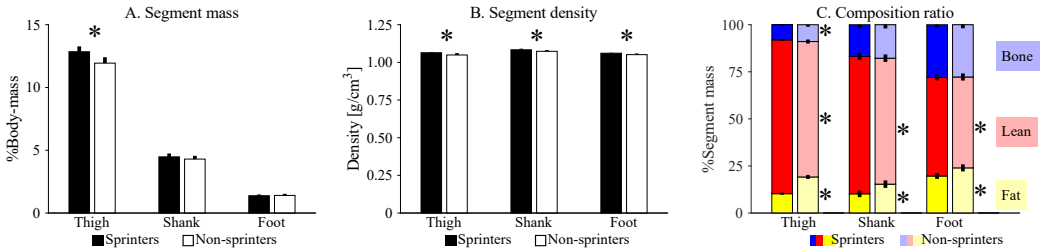

Fig. 3. Segment mass and its determinants of each lower-limb segment. Relative mass (A), density (B), and composition ratio (C) in each of the thigh, shank, and foot segments. Note: Bar graphs show mean and standard deviation. Asterisk (*) indicates a significant difference between sprinters and non-sprinters.

Table 2. Complete scaling coefficients to estimate segment inertia parameters in sprinters and non-sprinters.

Group	Segment	Length definition	Origin	Scaling factor for mass	Scaling factors for CoM position			Scaling factors for tensor of inertial					
				m [%]	x [%]	y [%]	z [%]	r_{xx} [%]	r_{yy} [%]	r_{zz} [%]	r_{xy} [%]	r_{yz} [%]	r_{zx} [%]
Sprinters													
	Thigh	HJC to KJC	HJC	12.9	0.6	-2.7	-44.0	27.7	27.4	13.4	1.8 (i)	5.7 (i)	6.1 (i)
	Shank	KJC to AJC	KJC	4.5	4.4	-4.1	-40.7	27.0	26.9	10.0	1.9 (i)	4.1	4.3 (i)
	Foot	CAL to MH_1–MH_5 midpoint	AJC	1.4	0.1	-31.0	-46.2	40.9	36.9	28.8	13.7	16.9 (i)	4.5
Non-sprinters													
	Thigh	HJC to KJC	HJC	11.9	1.6	-2.5	-43.9	27.9	27.7	13.0	1.8 (i)	5.7(i)	6.2 (i)
	Shank	KJC to AJC	KJC	4.3	4.5	-3.2	-40.9	27.6	27.5	9.9	2.7 (i)	2.6	3.4 (i)
	Foot	Cal to MH_1–MH_5 midpoint	AJC	1.4	0.6	-32.3	-43.9	42.3	40.3	24.9	10.1	16.4 (i)	6.3

Note: HJC: Hip joint center; KJC: Kip joint center; AJC: Ankle joint center; Cal: Calcaneus; MH1 (5): 1st (5th) Metatarsal Heads; CoM: Centre of mass;

Discussion

We found that sprinters have lower limbs with a larger relative mass but not a larger $\hat{I}^{\mathrm{Hip}}_{\mathrm{LowerLimb}}$ than non-sprinters. Although muscular adaptation, as previously demonstrated (Ema et al., 2018; Miller et al., 2020; Tottori et al., 2021), increases the force and power exertion capacity, the increase in mass due to hypertrophy has been speculated to make it difficult for the body to move in terms of inertia. However, we revealed that the mechanical difficulty in swinging the lower limb in sprinters does not increase relatively.

A notable difference in the segment mass between sprinters and non-sprinters was confirmed only in the thigh. Moment of inertia I is mechanically proportional to the square of the radius of gyration r:

$$I = mr^2. \tag{3}$$

For example, if same mass (e.g., 1 kg) is added to the thigh and shank in the sprinters in this study ($r_{\mathrm{Hip-to-ThighCoM}}$: 0.19 m; $r_{\mathrm{Hip-to-ShankCoM}}$: 0.60 m), the increase in lower-limb moment of inertia due to the added mass in the thigh (0.036 kg·m^2) is only 1/10 of that due to the added mass to the shank (0.360 kg·m^2). Based on simple mechanical laws, a small inertia can lead to both decreasing musculoskeletal demands and increasing body segment acceleration. Thus, bottom-heavy, top-light feature of the lower limb in sprinters can be an optimal solution for their performance, from the biomechanical perspective. All the thigh, shank, and foot segments in sprinters had greater lean tissue ratios, smaller fat tissue ratios, and greater densities than those in non-sprinters. The sprinter/non-sprinters ratios of segment density were very similar in all the three segments, including the thigh (approximately 101%). The sprinter/non-sprinters ratio of thigh density was smaller than that of the thigh mass (107.6%). These results indicate that the segment mass is more affected by the segment volume than the segment density. Furthermore, the bone mass ratio of the sprinters was nearly 10% smaller than that of non-sprinters only in the thigh, which is straightforward to interpret as the adaptation to sprinting involves an increase in segment volume only in the thigh. Taken together, we indicated that the lower-limb inertia properties in sprinters, having a larger relative mass but not a larger $\hat{I}^{\mathrm{Hip}}_{\mathrm{LowerLimb}}$, are the result of the hypertrophic potential being greater only in the thigh.

The proximal-segment-specific hypertrophic potential in the lower limb in sprinters is related to the muscle-tendon arrangement. The length ratio of the tendon to the muscle in a muscle-tendon unit (MTU) in humans has a large variation (0.01–11.25), which is generally because proximal MTUs have

shorter tendons compared to distal ones (Hoy et al., 1990). In a previous study (Kubo et al., 2011), the Achilles tendon thickness in sprinters and non-sprinters was similar (sprinters/non-sprinters: 98.6%), whereas the ankle plantar flexor muscle thicknesses were larger in sprinters than in non-sprinters (113.8–116.8%). A previous meta-analysis (Bohm et al., 2015) also showed a slight effect (weighted average effect size: 0.24) on the tendon hypertrophy in response to various types of exercise interventions. As such, the tendon tissue is hardly hypertrophic. Because of the difference in the hypertrophic potential between the muscle and tendon, the distal segment with a larger tendon length ratio results in a smaller volumetric (and mass) plasticity in the distal segment. Thus, it is suggested that the inter-segment differences in the hypertrophy are not a unique feature of sprinters, but the result of an adaptation potential in general in humans to explosive physical exercise. Regarding the significance of a larger tendon length ratio in the distal segment, a simulation study (Nagano et al., 2004) reported that a larger mechanical energy generation is obtained with a longer tendon when the mass is small and *vice versa*. This suggests the morphological advantage of the muscle-tendon arrangement in humans for executing explosive motion from the force/work exertion perspective. However, to the best of our knowledge, the morphological advantages for the inertial properties in humans have not been examined. The lower limb inertia properties found in sprinters, having a larger mass (related to muscle potential) but not a larger $\hat{I}_{\mathrm{LowerLimb}}^{\mathrm{Hip}}$, are beneficial both in preventing injury and improving performance. As discussed above, the increase in the lower-limb moment of inertia due to the added mass to the shank is 10-fold of that due to the added mass to the thigh; a smaller volumetric (and mass) plasticity in the distal segment is an important factor to keep the lower-limb moment of inertia small. Thus, our findings further add quantified evidence showing a novel significant advantage of the muscle-tendon arrangement for the adaptability to explosive (sprinting) motion from an inertial perspective.

We found differences in the normalized body segment inertia parameters (BSIPs), such as the radii of gyration, between sprinters and non-sprinters. Researchers have previously developed scaling coefficients to calculate BSIPs for motion analysis using direct measurements of elderly cadavers (Clauser et al., 1969) and *in vivo* medical imaging such as gamma-ray scanning (16), computed tomography (Huang and Suarez, 1983), or MRI (Cheng et al., 2000; Mungiole and Martin, 1990); however, these scaling factors do not adequately accommodate the effects of morphological adaptation on the inertial properties in athletes. We showed the complete scaling coefficients to

estimate the BSIPs of the sprinter's lower-limb segments, which provides sufficient scaling equations to calculate the hip, knee, and ankle joint dynamics. Although it is slightly outside the scope of this study, our data allow future studies to analyze motion in male sprinters more accurately.

Below, we discuss the methodological advantages and limitations of the present study. First, most of our MRI segmentation processes were computationally and automatically performed by the widely used standard Otsu's binarization algorithm (Otsu, 1996) on fat/water-separated images, leading to advantages in the methodological simplicity and robust results. Alternately, the landmark position coordinates were acquired by manual digitizing on the MRIs, having potential effects on the segment length used for data normalization. However, we acquired MRI images with a slice thickness of 2 mm, which is thinner than the previous studies examining inertia properties [for example, Sreenivasa et al. (2016): 6 mm–48 mm; Pearsall et al. (1994): 10 mm; Cheng et al. (2000): 20 mm]. We confirmed excellent repeatability of the segment lengths (ICC>0.96 and CV<1.5%); thus, the potential effect of manual digitizing on the segment length would not critically alter our results. Second, non-sprinters had similar body sizes as the average Japanese 20 year old males shown in the 2019 Japanese Government statistics (Government of Japan, 2020), while the sprinters were larger than the standard Japanese population, which might affect our conclusion. However, we assessed the dimensionless inertia parameters calculated according to Hof (1996) to eliminate the effect of body size. Although there were significant correlations between the absolute inertia and body size parameters, the dimensionless values (the relative mass and the normalized moment of inertia of the whole lower limb around the hip joint) did not correlate with the body size, suggesting that these values could reflect the individual differences in body shapes and mass distributions, thereby not being critically affected by the inter-group differences in the body size. Third, although we determined the sample size of each group as 12 based on *a priori* power analysis (see Methods section), we excluded one of the sprinter's data due to an error in the water/fat separation of his foot scan. However, the main findings regarding intergroup differences were statistically significant, which suggest that the exclusion did not critically affect our conclusion.

We examined only male participants. Generally, body composition has large sex differences (Bredella, 2017); therefore, our findings might not be directly applicable to females, which is an important future theme. It is also unclear whether our findings are applicable to the upper limbs. It has been suggested that high-speed throwing in the upper limbs is one of the factors for evolution in current

humans (Roach et al., 2013). It would not be surprising if humans also have morphological advantages in their upper limbs from an inertial perspective. Furthermore, unlike the lower limbs, which constantly support the body against gravity, the upper limbs, being free from such constant gravitational load, would reflect pure trainability in humans; the morphological adaptation in the upper limbs is an interesting future theme for understanding human plasticity in motor performance. Nevertheless, our findings regarding non-correspondence with an increase in lower-limb mass and moment of inertia in male sprinters open a novel perspective, inertia, for understanding human plasticity.

In conclusion, we demonstrate the lower-limb morphology in sprinters with a larger relative mass but with a not larger normalized moment of inertia around the hip comparing it to non-sprinters. This result suggests one of the practical advantages of human morphological characteristics–a larger tendon length ratio in the distal segment muscles–for their adaptation to explosive motor tasks, which provides a novel perspective to the literature for understanding human morphological adaptability.

Materials and Methods

Experimental design

We performed *a priori* power analysis for an independent *t*-test with the parameters of type I error; α=0.05, statistical power: 1-β=0.8, and effect size: Cohen's d=1.2 'very large' (Sawilowsky, 2009), which calculated the total sample size (n) as 24 (n=12 in each group). According to the power analysis, we recruited a total of 24 healthy males, including 12 well-trained (athletic career >7 years and 100 m best records: 10.44–10.83 s) sprinters and 12 non-sprinters who did not undertake resistance training or sports activities for at least 2 years. However, the data of one of the sprinters could not be analyzed because of an MRI error (fat/water separation error in the Dixon sequence) around the endpoint of the toe in the foot segment scan, and the main outcome data (i.e., the lower-limb mass and the moment of inertia around the hip joint) could not be calculated. Thus, we excluded this participant's data from the analysis. The analyzed participants were 11 sprinters (age: 20±2 yrs, height: 1.77±0.06 m; body mass: 68.2±4.4 kg, Mean±SD) and 12 non-sprinters (age: 23±3 yrs, height: 1.69±0.04 m; body mass: 58.6±4.5 kg). The purpose and experimental protocol of the study were explained to the participants and they provided written informed consent. The Human Research Ethics Committee at Waseda University, Japan approved the study protocol (reference number: 2019-174).

We used a 3.0 Tesla MR scanner (SIGNA Premier, GE Healthcare, Milwaukee, USA) to

obtain the MR scans. All lower limb segment scans were performed in the supine position. The 2-point 3D-dixon axial sequence, called "Lava-Flex" in GE Healthcare, was performed on the right thigh, shank, and foot segments ('Spacing-Between-Slices': 2 mm, 'Pixel-Spacing': [0.2930 0.2930] mm, Width×Height: 1024×1024 pixels, other detail information can be confirmed in the Supplemental material). Each scan of the thigh and shank had two sections because of the limitation in the length scanned in one section. The two sections of each thigh and the shank scans were taken continuously without changing the position on the MRI machine. In the MRI settings, the anteroposterior and mediolateral coordinates of the two consecutive scans coincided. To minimize the effect of magnetic field inhomogeneity on the Dixon sequence, the superoinferior ranges of the two scans overlapped by > 10 cm.

MRI processing

We analyzed the 16-bit depth MRI images using MATLAB 2019a (MathWorks, Natick, MA, USA). A flowchart of the segmentation procedure is presented in Fig. 4. To create a temporal body mask, we first created fat-only and water-only temporal binary images using a low intensity threshold. These binary images were added together, and the temporal body mask was defined by filling any internal holes in the added masks based on a binary morphology operation (Klingensmith et al., 2017). After creating the temporal body mask, we removed the pixel intensity in the unwanted areas (other than the range of interest, such as the part of the opposite leg segment included in the image). After that, we estimated and then homogenized the inhomogeneity field using a grayscale morphological closing operation with a large circular structure element (Klingensmith et al., 2017). The threshold for the foreground and background signal intensity of each of the fat-only and water-only images was determined using Otsu's method (Otsu, 1996), which created water-binary and fat-binary images. We created a definitive body mask by adding the two masks together and filling any internal holes with a binary morphology operation (Klingensmith et al., 2017). We classified each pixel as a fat tissue, lean (muscle or skin) tissue, or a background using water- and fat-binary images. For a slice having some voxels involved in both water- and fat-binary images, we further performed *k*-means clustering to classify the intensity of the voxels in the sum of the fat-only and water-only images (i.e., in-phase image) into three categories (fat tissue, lean tissue, or background), which were applied to the voxels involved in both the water-binary and fat-binary images.

The trabecular bone has MRI intensity characteristics similar to fat tissue because of the

279 yellow marrow (Sreenivasa et al., 2016), while the cortical bone is not brightened by MRI. These bone
280 tissues were classified as follows (Fig. 4):

281 Step 1. Search for a region inside the body mask region where the pixels classified as fat
282 tissue (trabecular bone in fact) are surrounded by pixels classified as background
283 (cortical bone in fact) and define them as trabecular bone and cortical bone.

284 Step 2. (When a bone cannot be explored in Step 1 and the trabecular bone is an
285 independent object in the fat-binary image), select and define the independent object in
286 the fat-only image as a trabecular bone.

287 Step 3. (When a trabecular bone was in contact with the outer fat tissue in the fat-binary
288 image and could not be defined in Steps 1 and 2) Manually draw a border with the fat
289 in the fat-only image or in-phase image using a pen tablet (Artist 15.6 Pro, XP-PEN,
290 Japan) and define the object as a trabecular bone.

291 Step 4. (After Steps 2 and 3) Define the pixels that surround the trabecular bone and are
292 classified as background (cortical bone in fact) as a cortical bone.

293 Step 5. Adjust the cortical bone if necessary (for example, if the tissue adjacent to the
294 cortical bone that is not depressed on MRI is considered to be a cortical bone).

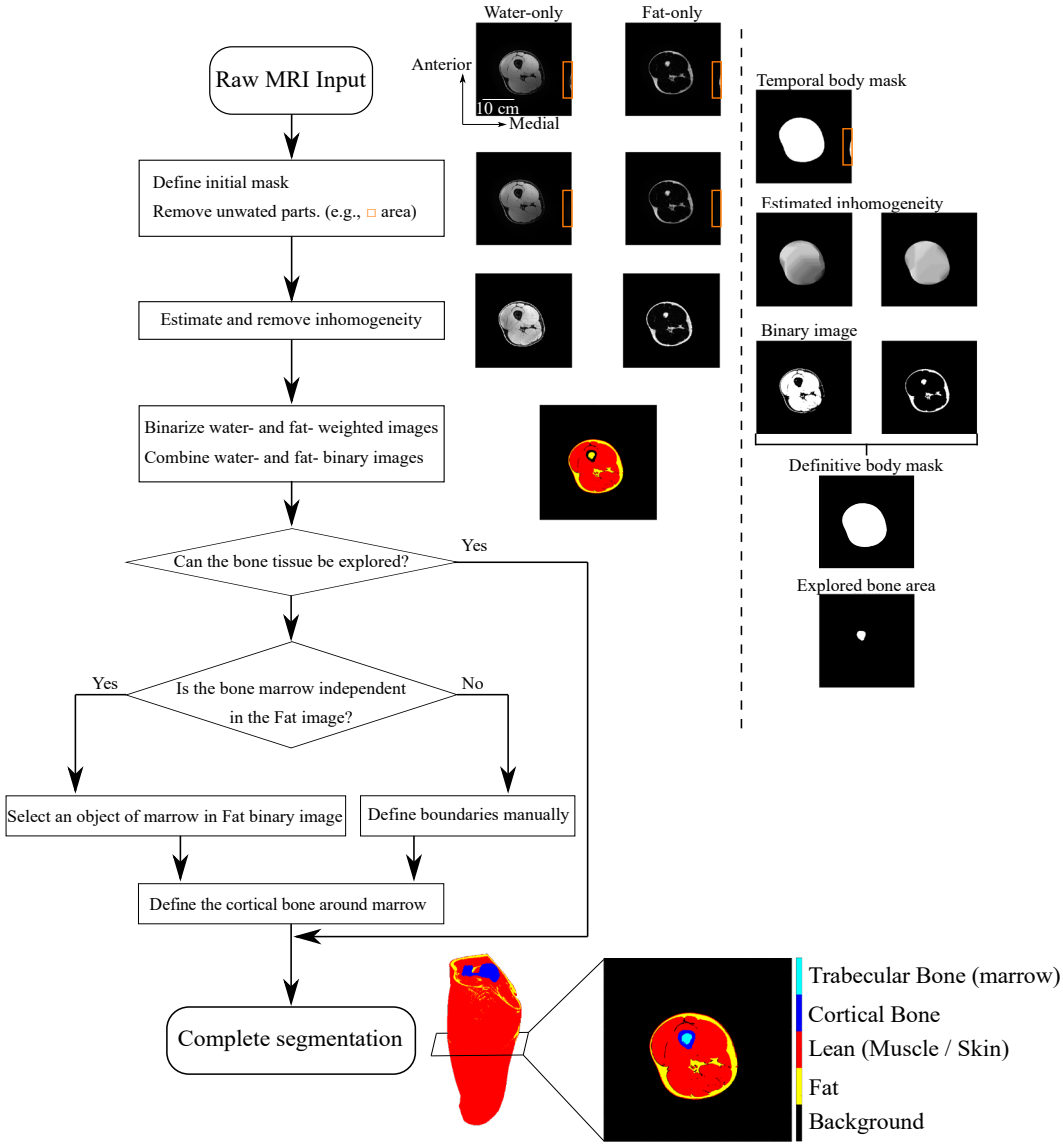

Fig. 4. Flowchart of the segmentation process based on water/fat separation images.

295

296 ***Data calculation***

297 The 3D coordinates of the anatomical landmarks (Table 3) on the MR coordinate system
298 were derived via manual digitizing in the 3D mode using the OsiriX software version 13 (Pixmeo,
299 Geneva, Switzerland) by an examiner. The examiner repeated the digitization of all landmarks from
300 eight participants for whom it had been >1 month following the first digitizing process to assess the
301 intra-examiner repeatability of manual digitizing.

302 The ankle joint in the foot and shank scans and the knee joint in the shank and thigh scans
303 were defined as the midpoints between the malleoli and the lateral and medial articular cleft of the
304 knee, respectively. The hip joint was defined using a least-squares calculation for a sphere fitting of 30
305 points distributed over the surface of the femoral head, similar to Harrington et al. (Harrington et al.,
306 2007). The ankle and knee boundary planes were defined as the horizontal planes passing those joint
307 locations (Fig. 5A). The hip joint boundary was defined by a plane 37º (Pearsall et al., 1996; Rossi et
308 al., 2013) vertical on the medial to the hip joint and a horizontal plane lateral to the hip joint (Pearsall et
309 al., 1994) (Fig. 5A). The lean and fat voxels outside of the border were excluded. The cortical and
310 trabecular bone voxel in that segment was retained even though it was outside the proximal and distal
311 borders. Bone voxels within the segment were retained even if they were outside the boundary, whereas
312 bone voxels in another segment were excluded even if they were inside the boundary.

313

Table 3. Anatomical landmarks to be acquired by manual digitizing.

Segments	Landmarks
Thigh	Surface of the femoral head (30 points)
	Lateral articular cleft between the femur and tibia condyle
	Medial articular cleft between the femur and tibia condyle
Shank	Lateral articular cleft between the femur and tibia condyle
	Medial articular cleft between the femur and tibia condyle
	Malleolus lateralis
	Malleolus medialis
Foot	Malleolus lateralis
	Malleolus medialis
	Calcaneus
	1st meta-tarsal heads
	5th meta-tarsal heads
	2nd toe tip

Note: Anatomical landmarks other than the femoral head were digitized closest points on the skin (i.e., points to which reflective markers can be attached when doing motion capture).

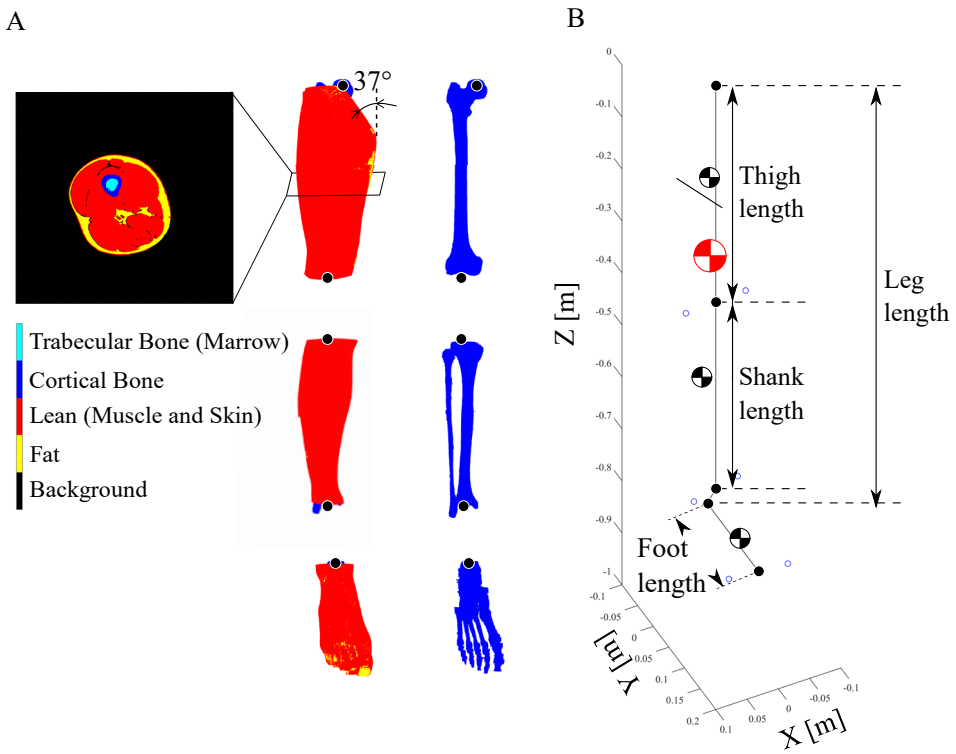

Fig. 5. A typical example of the constructed data. A three-dimensional constructed volume data of the thigh, shank and foot (A) and a stick picture created from three-dimensional position coordinates of the entire hypothetically constructed lower limb (B). Note: The origin of the hypothetical coordinates was at the hip joint center. The lower limb length was defined as the height difference between the hypothetical coordinates of the hip and calcaneus.

Based on the literature values (Huang and Wu, 1976; Martin et al., 1989), we defined the tissue density as:

$$\rho_k = [0.902\ 1.067\ 1.705\ 1.100], \tag{4}$$

where k=1,2,3,4 shows the tissues of fat, lean, cortical bone, and trabecular bone, respectively. The mass, m_s, volume V_s, density ρ_s, and position coordinates of the center of mass, $\begin{bmatrix} x_{s,\mathrm{CoM}} \\ y_{s,\mathrm{CoM}} \\ z_{s,\mathrm{CoM}} \end{bmatrix}$, of a segment s were calculated as

$$m_s = \sum_{k=1}^{4} \sum_{i=1}^{n_k} [(w^2 h)\rho_k] \tag{5}$$

$$V_s = \sum_{k=1}^{4} [(w^2 h) n_k] \tag{6}$$

$$\rho_s = \frac{m_s}{V_s} \tag{7}$$

$$\begin{bmatrix} x_{s,\mathrm{CoM}} \\ y_{s,\mathrm{CoM}} \\ z_{s,\mathrm{CoM}} \end{bmatrix} = \frac{1}{m_s} \sum_{k=1}^{4} \sum_{i=1}^{n_k} \left[(w^2 h) \rho_k \begin{bmatrix} x_i \\ y_i \\ z_i \end{bmatrix} \right] \tag{8}$$

where n_k is the number of voxels classified as the tissue k, w and h were the width ('Pixel-Spacing': 0.2930 mm) and height ('Spacing-Between-Slices': 2.0000 mm) of each voxel (i.e., $w^2 h$ is the volume of each voxel), and $\begin{bmatrix} x_i \\ y_i \\ z_i \end{bmatrix}$ is the position coordinate of the ith voxel, respectively.

Inertia tensor of segment s, $\boldsymbol{I}_s^{\mathbf{GCS}}$, was calculated as shown below:

$$\boldsymbol{I}_s^{\mathbf{GCS}} = \begin{bmatrix} \sum_{i=1}^{n} \left[I_{x_i} + m_i ({y_i}^2 + {z_i}^2) \right] & -\sum_{i=1}^{n} (m_i x_i y_i) & -\sum_{i=1}^{n} (m_i z_i x_i) \\ -\sum_{i=1}^{n} (m_i x_i y_i) & \sum_{i=1}^{n} \left[I_{y_i} + m_i ({z_i}^2 + {x_i}^2) \right] & -\sum_{i=1}^{n} (m_i y_i z_i) \\ -\sum_{i=1}^{n} (m_i z_i x_i) & -\sum_{i=1}^{n} (m_i y_i z_i) & \sum_{i=1}^{n} \left[I_{z_i} + m_i ({x_i}^2 + {y_i}^2) \right] \end{bmatrix} \tag{9}$$

where m_i is the mass of ith voxel, I_{x_i} I_{y_i} and I_{z_i} were the moments of inertia of each voxel and were calculated as follows.

$$I_{x_i} = I_{y_i} = \frac{m_i (w^2 + h^2)}{12} \text{ and } I_{z_i} = \frac{m_i (2w^2)}{12} \tag{10}$$

A right-handed orthogonal segment coordinate system (SCS) was fixed at each of the thigh, shank, and foot segments using the 3D coordinates of landmarks. This definition was consistent with that used by Sado et al. (2022, 2017). We calculated the inertia tensor in each SCS ($\boldsymbol{I}_s^{\mathbf{SCS}}$) as follows:

$$\boldsymbol{I}_s^{\mathbf{SCS}} = \boldsymbol{R}_s{}' \boldsymbol{I}_s^{\mathbf{GCS}} \boldsymbol{R}_s \tag{11}$$

where $\boldsymbol{R}_s$ is the rotational transformation matrix from the SCS to the GCS of segment s. Note that the principal axes of the segments are not consistent with the axes of the SCSs (Dumas et al., 2007); thus, $\boldsymbol{I}_s^{\mathbf{SCS}}$ is not in the form of a diagonal matrix, which is similar to Dumas et al. (2007), considering the differences between the SCS axes and the inertial principal axes.

We hypothetically created the lower-limb data in an anatomical position from the 3D coordinates in the MRI coordinate system of the thigh, shank, and foot using hierarchically constructed coordinates with the hip as the origin (Fig. 5B). In this hypothetical creation, the ***x***-axis directions of their SCSs were consistent with each other. We then calculated $I_{\mathrm{LowerLimb}}^{\mathrm{Hip}}$ in the data of this hypothetical anatomical position as

$$I_{\text{Lowerlimb}}^{\text{Hip}} = \sum_{s=1}^{3} \left\{ {I_s^{\text{SCS}}}_{xx} + m_s \left(\left| y_s - y_{\text{Hip}} \right|^2 + \left| z_s - z_{\text{Hip}} \right|^2 \right) \right\} \tag{12}$$

where ${I_s^{\text{SCS}}}_{xx}$ is the moment of inertia of the segment around its CoM, y_s, y_{Hip}, z_s and z_{Hip} are the anteroposterior or superoinferior coordinates of the CoM of segment $\boldsymbol{s}$ or the hip joint in a hypothetically created coordinate. In this coordinate system, the origin is set at the hip joint; thus, y_{Hip}, and z_{Hip} are equal to zero.

The segment and the lower-limb masses were expressed relative to the whole-body mass. Both the products and the moments of inertia of each segment were expressed relative to the segment length l_s and the segment mass m_s. For example, the moment of inertia of segment s around the $\boldsymbol{x}$-axis is

$$r_{s_{xx}} = \frac{\sqrt{\frac{{I_s^{\text{SCS}}}_{xx}}{m_s}}}{l_s} \tag{13}$$

The segment lengths were defined as the Euclidean distances between the proximal and distal joint locations (Fig. 5B). Using the scaling method of gait data established by Hof (Hof, 1996), we normalized $I_{\text{LowerLimb}}^{\text{Hip}}$ by the lower-limb length ($l_{\text{Lowerlimb}}$) and the whole-body mass (m_{body}) as:

$$\hat{I}_{\text{LowerLimb}}^{\text{Hip}} = \frac{I_{\text{LowerLimb}}^{\text{Hip}}}{m_{\text{body}} {l_{\text{Lowerlimb}}}^2} \tag{14}$$

where $l_{\text{Lowerlimb}}$ is the height difference between the hip joint center and calcaneus in the hypothetically created coordinates (Fig.5B).

Statistical analysis

We used MATLAB 2019a for statistical analysis. We used ICCs and CVs to assess the repeatability of the examiners' manual-digitising-basis segment lengths. The ICCs can be interpreted as good (>0.75) or excellent (>0.90) (37). After normality confirmation using the Jarque-Bera test, we calculated the Pearson's correlation coefficient (*r*) to confirm the effect of body size on the lower-limb inertia properties.

We tested the significance of the intergroup differences using an independent *t*-test. The statistical significance was set at 0.05. The effect size of each *t*-test was determined using Cohen's *d* (Cohen, 1988) with classification as small (≤0.49), medium (0.50–0.79), large (0.80–1.19), very large (1.20–1.99), and huge (≥2.00) (Sawilowsky, 2009).

Acknowledgements

We would like to thank Dr. Gaku Kakehata for his help in participant recruitment.

References

Balshaw TG, Maden-Wilkinson TM, Massey GJ, Folland JP. 2021. The Human Muscle Size and Strength Relationship: Effects of Architecture, Muscle Force, and Measurement Location. *Med Sci Sport Exerc* **Publish Ah**.

Bohm S, Mersmann F, Arampatzis A. 2015. Human tendon adaptation in response to mechanical loading: a systematic review and meta-analysis of exercise intervention studies on healthy adults. *Sport Med - Open* **1**. doi:10.1186/s40798-015-0009-9

Bramble DM, Lieberman DE. 2004. Endurance running and the evolution of Homo. *Nature* **432**:345–352. doi:10.1038/nature03052

Bredella MA. 2017. Sex Differences in Body Composition BT - Sex and Gender Factors Affecting Metabolic Homeostasis, Diabetes and Obesity In: Mauvais-Jarvis F, editor. Cham: Springer International Publishing. pp. 9–27. doi:10.1007/978-3-319-70178-3_2

Cheng CK, Chen HH, Chen CS, Lee CL, Chen CY. 2000. Segment inertial properties of Chinese adults determined from magnetic resonance imaging. *Clin Biomech* **15**:559–566. doi:10.1016/S0268-0033(00)00016-4

Clauser CE, McConville JT, Young JW. 1969. Weight, Volume, and Center of Mass of Segments of the Human Body. *Natl Tech Inf Serv* 1–112. doi:AMRL-TR- 69-70 (AD 710 622)

Cohen J. 1988. Statistical power analysis for the behavioral sciences, 2nd ed, Statistical Power Analysis for the Behavioral Sciences. Hillsdale: Lawrence Earlbaum Associates. doi:10.1234/12345678

de Leva P. 1996. Adjustments to Zatsiorsky-Seluyanov's segment inertia parameters. *J Biomech* **29**:1223–1230. doi:10.1016/0021-9290(95)00178-6

Dorn TW, Schache AG, Pandy MG. 2012. Muscular strategy shift in human running: dependence of running speed on hip and ankle muscle performance. *J Exp Biol* **215**:1944–56. doi:10.1242/jeb.064527

Dumas R, Chèze L, Verriest JP. 2007. Adjustments to McConville et al. and Young et al. body segment inertial parameters. *J Biomech* **40**:543–553. doi:10.1016/j.jbiomech.2006.02.013

Ema R, Sakaguchi M, Kawakami Y. 2018. Thigh and Psoas Major Muscularity and Its Relation to

Running Mechanics in Sprinters. *Med Sci Sport Exerc* **50**:2085–2091. doi:10.1249/MSS.0000000000001678

Fukunaga T, Miyatani M, Tachi M, Kouzaki M, Kawakami Y, Kanehisa H. 2001. Muscle volume is a major determinant of joint torque in humans. *Acta Physiol Scand* **172**:249–255. doi:10.1046/j.1365-201x.2001.00867.x

Government of Japan. 2020. e-Stat: Portal Site of Official Statistics of Japan. https://www.e-stat.go.jp/en

Harrington ME, Zavatsky AB, Lawson SEM, Yuan Z, Theologis TN. 2007. Prediction of the hip joint centre in adults, children, and patients with cerebral palsy based on magnetic resonance imaging. *J Biomech* **40**:595–602. doi:10.1016/j.jbiomech.2006.02.003

Hof AL. 1996. Scaling gait data to body size. *Gait Posture* **4**:222–223. doi:10.1016/0966-6362(95)01057-2

Hoy MG, Zajac FE, Gordon ME. 1990. A musculoskeletal model of the human lower extremity: The effect of muscle, tendon, and moment arm on the moment-angle relationship of musculotendon actuators at the hip, knee, and ankle. *J Biomech* **23**:157–169. doi:10.1016/0021-9290(90)90349-8

Huang HK, Suarez FR. 1983. Evaluation of cross-sectional geometry and mass density distributions of humans and laboratory animals using computerized tomography. *J Biomech* **16**:821–832. doi:10.1016/0021-9290(83)90006-4

Huang HK, Wu SC. 1976. The evaluation of mass densities of the human body in vivi from CT Scans. *Comput Biol Med* **6**:337–343. doi:10.1016/0010-4825(76)90070-6

Japan Sports Agency. 2021. The Report of FY 2020 Survey on Physical Strength and Athletic Performance.

Klingensmith JD, Elliott AL, Fernandez-del-Valle M, Mitra S. 2017. Automated segmentation of cardiac adipose tissue in Dixon magnetic resonance images. *J Biomed Graph Comput* **8**:1. doi:10.5430/jbgc.v8n1p1

Kubo K, Ikebukuro T, Yata H, Tomita M, Okada M. 2011. Morphological and mechanical properties of muscle and tendon in highly trained sprinters. *J Appl Biomech* **27**:336–344.

Martin PE, Mungiole M, Maezke MW, Longhill JM. 1989. The use of magnetic resonance imaging for measuring segment inertial propertierties. *J Biomech* **22**:367–376.

Miller R, Balshaw TG, Massey GJ, Maeo S, Lanza MB, Johnston M, Allen SJ, Folland JP. 2020. The

Muscle Morphology of Elite Sprint Running. *Med Sci Sport Exerc* **53**:804–815. doi:10.1249/mss.0000000000002522

Mungiole M, Martin PE. 1990. Estimating segment inertial properties: Comparison of magnetic resonance imaging with existing methods. *J Biomech* **23**:1039–1046. doi:10.1016/0021-9290(90)90319-X

Nagano A, Komura T, Fukashiro S. 2004. Effects of the length ratio between the contractile element and the series elastic element on an explosive muscular performance. *J Electromyogr Kinesiol* **14**:197–203. doi:10.1016/S1050-6411(03)00085-3

O'Brien TD, Reeves ND, Baltzopoulos V, Jones DA, Maganaris CN. 2009. Strong relationships exist between muscle volume, joint power and whole-body external mechanical power in adults and children. *Exp Physiol* **94**:731–738. doi:10.1113/expphysiol.2008.045062

Otsu N. 1996. A threshold selection method from gray-level histograms. *IEEE Trans Syst Man Cybern* **9**:62–66.

Pearsall DJ, Reid JG, Livingston L a. 1996. Segmental inertial parameters of the human trunk as determined from computed tomography. *Ann Biomed Eng* **24**:198–210. doi:10.1007/BF02667349

Pearsall DJ, Reid JG, Ross R. 1994. Inertial properties of the human trunk of males determined from magnetic resonance imaging. *Ann Biomed Eng* **22**:692–706. doi:10.1007/BF02368294

Roach NT, Venkadesan M, Rainbow MJ, Lieberman DE. 2013. Elastic energy storage in the shoulder and the evolution of high-speed throwing in Homo. *Nature* **498**:483–6. doi:10.1038/nature12267

Rossi M, Lyttle A, El-Sallam A, Benjanuvatra N, Blanksby B. 2013. Body segment inertial parameters of elite swimmers using DXA and indirect methods. *J Sport Sci Med* **12**:761–775.

Sado N, Yoshioka S, Fukashiro S. 2022. Curved approach in high jump induces greater jumping height without greater joint kinetic exertions than straight approach. *Med Sci Sport Exerc* **54**:120–128. doi:10.1249/mss.0000000000002761

Sado N, Yoshioka S, Fukashiro S. 2017. A non-orthogonal joint coordinate system for the calculation of anatomically practical joint torque power in three-dimensional hip joint motion. *Int J Sport Heal Sci* **15**:111–119. doi:10.5432/ijshs.201712

Sawilowsky SS. 2009. New Effect Size Rules of Thumb. *J Mod Appl Stat Methods* **8**:597–599. doi:10.22237/jmasm/1257035100

Schache AG, Blanch PD, Dorn TW, Brown NAT, Rosemond D, Pandy MG. 2011. Effect of running

speed on lower limb joint kinetics. *Med Sci Sports Exerc* **43**:1260–1271. doi:10.1249/MSS.0b013e3182084929

Shan G, Bohn C. 2003. Anthropometrical data and coefficients of regression related to gender and race. *Appl Ergon* **34**:327–337. doi:10.1016/S0003-6870(03)00040-1

Sreenivasa M, Chamorro CJG, Gonzalez-Alvarado D, Rettig O, Wolf SI. 2016. Patient-specific bone geometry and segment inertia from MRI images for model-based analysis of pathological gait. *J Biomech* **49**:1918–1925. doi:10.1016/j.jbiomech.2016.05.001

Takahashi K, Kamibayashi K, Wakahara T. 2021. Muscle size of individual hip extensors in sprint runners: Its relation to spatiotemporal variables and sprint velocity during maximal velocity sprinting. *PLoS One* **16**:1–12. doi:10.1371/journal.pone.0249670

Tottori N, Suga T, Miyake Y, Tsuchikane R, Tanaka T, Terada M, Otsuka M, Nagano A, Fujita S, Isaka T. 2021. Trunk and lower limb muscularity in sprinters: what are the specific muscles for superior sprint performance? *BMC Res Notes* **14**:10–15. doi:10.1186/s13104-021-05487-x

Young NM, Wagner GP, Hallgrímsson B. 2010. Development and the evolvability of human limbs. *Proc Natl Acad Sci U S A* **107**:3400–5. doi:10.1073/pnas.0911856107